applied sciences

MDPI

Article

Study on the Influence of Triangular Groove Structure on Steady-State Flow Force Compensation Characteristics

Ruichuan Li [1], Xinkai Ding [1,*], Jianghai Lin [2], Feng Chi [3], Jikang Xu [1,*], Yi Cheng [1], Jilu Liu [1] and Qi Liu [1]

[1] College of Mechanical and Automotive Engineering, Shandong Academy of Sciences, Qilu University of Technology, Jinan 250000, China; liruichuan@qlu.edu.cn (R.L.); 1043119053@stu.qlu.edu.cn (Y.C.); 10431200137@stu.qlu.edu.cn (J.L.); 10431200035@stu.qlu.edu.cn (Q.L.)
[2] Shandong Machinery Design & Research Institute, Jinan 250000, China; linjianghai@qlu.edu.cn
[3] Shandong Lingong Construction Machinery Co., Ltd., Linyi 276000, China; feng.chi@sdlg.com.cn
* Correspondence: 10431200080@stu.qlu.edu.cn (X.D.); 10431200081@stu.qlu.edu.cn (J.X.)

Abstract: In this study, a structurally improved spool was designed. The diameter of one side of the spool stem was reduced, making the spool stem into a rounded table shape. A triangular groove was circumscribed on the step and on the same side. After liquid flow was guided through the triangular groove, the flow direction changed. A flow component in the negative direction was generated, which reversely impacted the liquid flow in the positive direction. The liquid flow angle at the outlet increased; that is, jet angle increased and flow force decreased. The simulation results show that, increasing the depth, H, of the triangular groove has a positive effect on flow-force compensation and was conducive to the stability of the valve core. Properly increasing the groove's bottom diameter, D_1, of the triangular groove was conducive to the stability of the spool, but when D_1 was too large, the flow force increased. The experimental results are consistent with the simulation results, which proves that the improved structure can effectively reduce the flow force of the spool.

Keywords: steady flow force; diversion; jet angle; compensation characteristics

Citation: Li, R.; Ding, X.; Lin, J.; Chi, F.; Xu, J.; Cheng, Y.; Liu, J.; Liu, Q. Study on the Influence of Triangular Groove Structure on Steady-State Flow Force Compensation Characteristics. *Appl. Sci.* **2021**, *11*, 11354. https://doi.org/10.3390/app112311354

Academic Editor: Cesare Biserni

Received: 6 November 2021
Accepted: 25 November 2021
Published: 30 November 2021

1. Introduction

Hydraulic technology is widely used in modern industry because of its remarkable characteristics of large power–weight ratio, high control accuracy and good stability [1,2]. The design and optimization of hydraulic components is an important link in improving hydraulic technology [3,4]. A hydraulic control element is one of the basic components of a hydraulic system. It mainly refers to hydraulic control valves, including pressure valves, flow valves and direction valves, though slide and pilot valves are commonly used. The working principle is to control the flow and flow direction of fluid through the relative movement of the valve core and the valve body, and directly or indirectly controlling the movement of an actuator [5]. As important parts of a hydraulic system, the static and dynamic characteristics of hydraulic valves have an important impact on the stability of a hydraulic system [6,7]. In recent years, flow force has become a research hotspot of scholars the world over. Flow force is divided into transient flow force and steady-state flow force, in which steady-state flow force has a great influence on the static characteristics of hydraulic valves. As early as the 1950s, Lee and Blackburn [8] researched steady-state flow forces. Amirante et al. [9,10] analyzed the driving forces on a 4/3 hydraulic open center directional control valve. The valve was tested with different pump flow rates, as well as with different pressure drops. Their results showed important differences between an open-center valve and a closed-center one. Rannow and Li [11] proposed a soft switching approach to eliminate the majority of valves' transition losses. The simulation results showed that the soft switching approach has the potential to improve the efficiency of on/off-controlled systems. They studied the hydrodynamics of a hydraulic valve based on one-dimensional and three-dimensional CFD modeling methods to analyze the flow-force,

pressure and velocity characteristics of hydraulic valve. Ye et al. [12] clarified the effects of a grooved shape on flow characteristics through computational fluid dynamics (CFD) and experimental investigations. They furthermore analyzed the changes of restricted locations along with the openings to calculate the flow areas of the notches. The discharge coefficient, as a function of groove geometry, flow condition, fitting coefficients and its stable value, was deduced, proving to be quite consistent in their experimental result. Lu [13,14] researched the effects of radial flow force and static pressure upon the lateral force. The jet angle was discovered not only to be related to the annular orifice opening and gap clearance but was also influenced by the flow direction and control-surface profile.

Lü et al. [15] applied a numerical simulation method based on the flow-solid interaction (FSI) to observe the variation of the jet force when the flapper is moving. They established the relationship between the movement of the flapper, the flow field distribution, the jet force and the inlet pressure. Lu et al. [16] the stability of two-dimensional (2D) servo valve and its influencing factors and concluded that the steady-state flow force generated by fluid flowing through the spiral valve port belongs to space force which is not conducive to the stability of the valve core. Wang et al. [17] established the dynamics characteristics of a poppet relief valve containing both a transient flow force and a steady flow force. They observed that the flow force had an important impact on the stability of the valve. Qu et al. [18] built a mathematical flow-force model of converged flow valves and studied the influences of different fit clearances on the steady-state flow forces of valves. The results showed that the fit clearance had an important influence on valves' steady-state flow force. Zhang et al. [19] established a three-dimensional model of computational fluid dynamics by using CFD-ACE + software. The instantaneous flow field, spool displacement, flow force and deformation of the hydraulic control directional valve with three throttling structures were compared. The above literature shows that flow force has an important impact on the stability of hydraulic valves. In order to ensure the operability and accuracy of hydraulic valve, flow force must be compensated. Herakovic et al. [20] defined the structure of a slide spool and a spool sleeve in detail and used CFD simulation calculation to reduce the steady-state flow force by changing the geometry of the spool sleeve and spool. Altare et al. [21] studied the 3D and 0D simulation of a conical popped pressure-relief valve with flow-force compensation and created a dynamic model. The model was able to determine the equilibrium position of the poppet in order to estimate the regulated pressure as function of the flow rate. They also studied influence of the deflector geometry on the opening force to realize the compensation of flow force. Tan et al. [22] proposed a method aimed at reducing the steady-state axial flow force working on the main spool of a diverged flow cartridge proportional valve; they found a rule governing how these parameters influence flow force by a series of computational fluid dynamics (CFD) simulations. Roberto and Massimo [23] studied the effect of poppet geometry on the flow-pressure characteristics of a direct-acting pressure-relief valve. A dynamic 3D-CFD model was built in ANSYS Fluent to predict the flow-pressure characteristics of the valve for different spring preload settings and deflector geometries. Then, they calculated the effect of the geometric parameters of the poppet and optimized the cone angle and the position of the deflector to compensate for the flow force. Zhang and Li [24] proposed machining an annular groove on a spool core to compensate for flow force, and analyzed the influence of the depth of the spool sleeve's sunk groove, the depth and width of the annular groove of the spool core and other factors of its compensation characteristics. Dong and Fu [25] used the Fluent simulation software to explore the effects of groove depth and included angle of the throttling groove and the deflection the angle between the V-groove and the symmetrical plane of the spool sleeve on the steady-state flow force acting on the spool, as well as the flow characteristics of the spool port.

In this paper, the flow force of a hydraulic valve is analyzed, and an improved method of spooling is proposed. Based on the force and jet angle of the spool, the influence law of the structural parameters of the improved spool on flow-force compensation characteristics

is further studied through simulation, and an experimental platform is built to verify the simulation results.

2. Flow Force Analysis

Figure 1 shows the stress on the spool, and the flow force can be expressed as follows:

$$F_F = F_{\tau_{rod}} + F_s + F_d \tag{1}$$

where F_F is flow force. $F_{\tau_{rod}}$ is the viscous force generated by fluid acting on the spool. F_s is the static force generated by fluid acting on the spool. F_d is the dynamic force generated by fluid acting on the spool.

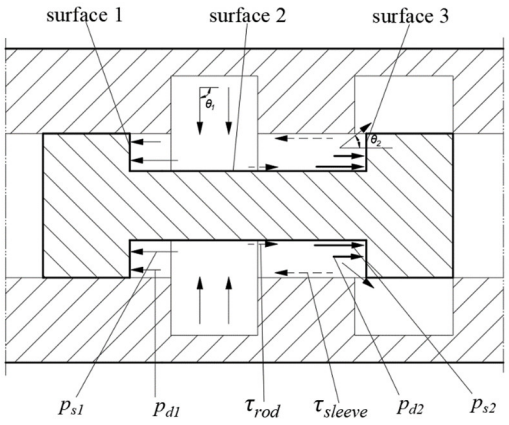

Figure 1. Stress of the spool.

Selecting 'right' as the positive direction, $F_{\tau_{rod}}$, F_s and F_d can be expressed as follows:

$$F_{\tau_{rod}} = \iint_{A_{rod}} \tau_{rod} dA \tag{2}$$

$$F_s = \iint_{A_r} p_{s2} dA - \iint_{A_l} p_{s1} dA \tag{3}$$

$$F_d = \iint_{A_r} p_{d2} dA - \iint_{A_l} p_{d1} dA \tag{4}$$

where τ_{rod} is the shear force generated by fluid acting on the spool stem. p_{s1} and p_{s2} are the static pressure generated by fluid acting on the left shoulder surface 1 and the right shoulder surface 3 of the spool. p_{d1} and p_{d2} are dynamic pressure generated by the fluid acting on the left shoulder surface 1 and the right shoulder surface 3 of the spool. A_{rod} is the surface area of the spool stem. A_l and A_r are the areas of the left shoulder surface 1 and the right shoulder surface 3 of the spool.

So, the flow force can be expressed as follows:

$$F_F = \iint_{A_{rod}} \tau_{rod} dA + \iint_{A_r} p_{s2} dA - \iint_{A_l} p_{s1} dA + \iint_{A_r} p_{d2} dA - \iint_{A_l} p_{d1} dA \tag{5}$$

In this paper, the forces of the spool in the steady state are studied, and the transient flow force is ignored; that is, the dynamic forces generated by the fluid acting on the spool are ignored. The flow force of the spool can be expressed as follows:

$$F_F = \iint_{A_{rod}} \tau_{rod} dA + \iint_{A_r} p_{s2} dA - \iint_{A_l} p_{s1} dA \tag{6}$$

Flow force can also be calculated by momentum theorem. Taking the fluid as the research object, the fluid is subjected to two forces: the force exerted by the spool sleeve and the force exerted by the spool. The force that the spool enacts on the fluid and the force that the fluid enacts on the spool are the action and reaction forces. Therefore, the force acting on the fluid can be expressed as follows:

$$F_{liquid} = F_{sleeve} - F_F \tag{7}$$

where F_{liquid} is the force on the fluid. F_{sleeve} is the force exerted by the sleeve on the fluid.

F_{sleeve} can be expressed as follows:

$$F_{sleeve} = \iint\limits_{A_{sleeve}} \tau_{sleeve} dA \approx \alpha \mu L q \tag{8}$$

where τ_{sleeve} is the shear force generated by the spool sleeve acting on the fluid. A_{sleeve} is the contact area between the sleeve and the fluid. α, u and L are the geometry coefficient of runner, fluid viscosity and effective length of the fluid, respectively. q is flow rate.

From the momentum conservation theorem:

$$F_{liquid} = \frac{d}{dt} \iiint\limits_{C.V.} \rho v_x dV + \iint\limits_{A_i} \rho v_x v \times i dA + \iint\limits_{A_o} \rho v_x v \times (-i) dA \tag{9}$$

where ρ is fluid density, v is fluid velocity, v_x is fluid axial velocity, i is the left unit normal vector, A_i is the inlet area, A_o is the outlet area.

Ignoring the transient flow force, the following results can be obtained as follows:

$$F_{liquid} = \rho q v_2 \cos\theta_2 - \rho q v_1 \cos\theta_1 \tag{10}$$

where v_1 and v_2 are the average speeds at the inlet and outlet. θ_1 and θ_2 are the jet angles at the inlet and outlet. Steady-state flow force can be expressed as follows:

$$F_F = F_{sleeve} - F_{liquid} = \alpha \mu L q + \rho q v_1 \cos\theta_1 - \rho q v_2 \cos\theta_2 \tag{11}$$

According to the above derivation, the steady-state flow force is in the direction of closing the valve, that is, the negative direction. The steady-state flow force value depends on the forces on the left and right shoulder of the spool and the side of the spool stem. The jet angle at the outlet also affects the steady-state flow force.

3. Modeling and Simulation

The improved spool is shown in Figure 2. In this paper, the diameter of the right spool stem is reduced on the basis of the original spool, so that the spool stem is in the shape of a round platform. A triangular groove is circumscribed on the right step, which is composed of surface 3 and surface 4. After part of the liquid flow is diverted through surface 3 and surface 4, the flow direction changes, that is, a leftward flow component is generated. This part of the liquid flow reversely impacts the liquid flow flowing to the right, which increases the jet angle at the outlet and reduces the flow force. As the diameter on the right side of the spool stem is reduced to form a round platform, the space on the right side of the spool stem is larger. This allows more fluid to flow through surface 3 and surface 4, further reducing the flow force. As shown in Figure 3, the main structural parameters of the improved spool are the right spool stem's end diameter, D, the triangular groove's bottom diameter, D_1, and the groove depth, H.

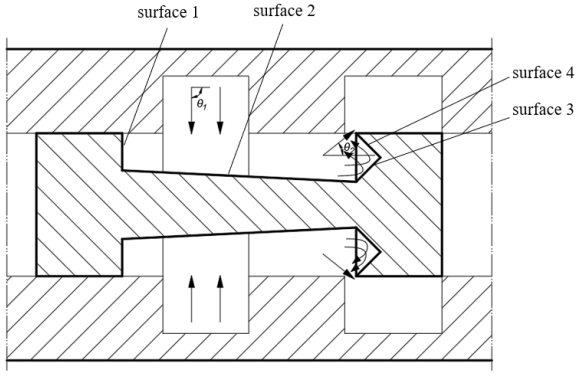

Figure 2. Improved spool compensation principle.

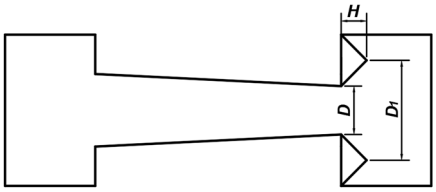

Figure 3. Structural parameters of the improved spool.

The three-dimensional model was established in SolidWorks and imported into ANSYS/Fluent to simulate the fluid domain. In this paper, the initial parameters are D = 8 mm, H = 4 mm, D_1 = 16 mm. The diameter of the unmodified stem is 12 mm. Reynolds number is 2351. There are three turbulence models K-ε, K-ω, and Reynolds stress in ANSYS/Fluent. K-ε model is the most widely used turbulence model in the research of hydraulic valve. Based on this model, the valve is simulated and analyzed in this paper. Turbulent kinetic energy, K, and dissipation, ε, can be derived from the migration equation, as follows:

$$\frac{\partial}{\partial \mathrm{t}}(\rho k) + \frac{\partial}{\partial x_i}(\rho k u_i) = \frac{\partial}{\partial x_j}[(\mu + \frac{\mu_t}{\sigma_k})\frac{\partial k}{\partial x_j}] + G_k + G_b - \rho\varepsilon - Y_M + S_k \tag{12}$$

$$\frac{\partial}{\partial \mathrm{t}}(\rho \varepsilon) + \frac{\partial}{\partial x_i}(\rho \varepsilon u_i) = \frac{\partial}{\partial x_j}[(\mu + \frac{\mu_t}{\sigma_\varepsilon})\frac{\partial_\varepsilon}{\partial x_j}] + C_{1\varepsilon}\frac{\varepsilon}{k}(G_k + C_{3\varepsilon}G_b) - C_{2\varepsilon}\rho\frac{\varepsilon^2}{k} + S_\varepsilon \tag{13}$$

where G_k is the turbulent kinetic energy generated by the average velocity gradient. G_b is the turbulent kinetic energy generated by liquid buoyancy. Y_M is the fluctuation expansion of the overall dissipation rate in the compressible turbulent flow. $C_{1\varepsilon}$, $C_{2\varepsilon}$ and $C_{3\varepsilon}$ are model constants. σ_k and σ_ε are the turbulent Prandtl number of k and ε, S_k and S_ε are user-defined values. μ_t is turbulent viscosity, which can be expressed as follows:

$$\mu_t = \rho C_\mu \frac{k^2}{\varepsilon} \tag{14}$$

In this paper, the form of the pressure inlet and pressure outlet are adopted; the inlet pressure is 3 MPa and the outlet pressure is 0.5 MPa, and the fit clearance between the spool and the spool sleeve is ignored. The fluid density is 870 $\mathrm{kg \cdot m^{-3}}$. The dynamic viscosity is 0.04 $\mathrm{kg \cdot m^{-1} \cdot s^{-1}}$.

4. Simulation Results and Analysis

4.1. When H and D_1 Remain Unchanged, the Influence of D Changes the Flow Force

When the fixed values H = 4 mm, D_1 = 16 mm, spool opening x_v = 1 mm are unchanged, D changes within the range of 4–12 mm, where every 2 mm is a measuring point. As shown in Figure 4, when D changes within the range of 4–12 mm, the variation range of the force on surface 1 is very small, and the maximum difference is only 0.45 N compared with the

unimproved spool. The direction of the force on surface 1 is vertical surface 1 to the left. This is because the liquid flow state at the left end of the spool and the spatial distribution of surface 1 are basically not affected by the change of the diameter at the right end, and the pressure on the left side remains basically unchanged. As shown in Figure 5, as the diameter of the right end decreases, the force on surface 2 gradually increases, and the force direction is negative, that is, in the spool's closing direction. This is because the diameters of the left and right ends of the spool are different, forming a certain stress area on the side surface of the spool stem, resulting in the leftward force. With decreasing diameter, the force on the surface 2 increases.

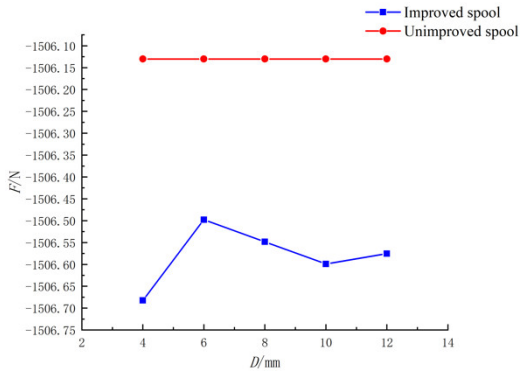

Figure 4. Force on surface 1 of two spools.

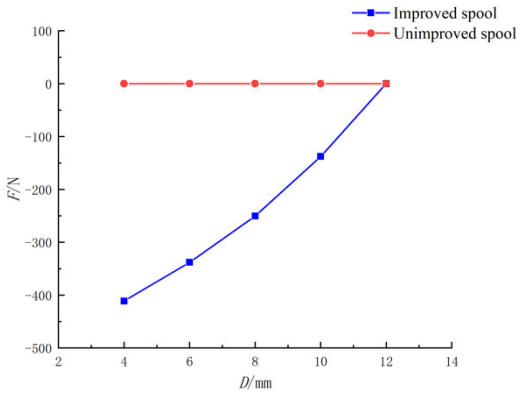

Figure 5. Force on surface 2 of two spools.

The forces on the improved spool surface 3 and surface 4 are shown in Figure 6. The force on the surface 3 of the improved spool increases with the decrease of diameter, D. This is because when H and D_1 remain unchanged, the smaller the D, the greater the included angle between surface 3 and the horizontal plane, and the greater the impact of liquid flow on plane 3, that is, the greater the force. At the same time, changing the diameter will not affect the spatial distribution of surface 4, and the impact of fluid on surface 4 will not change greatly, that is, the force on surface 4 is basically unchanged. As can be seen in Figure 6, the sum of the forces on surface 3 and surface 4 of the improved spool is greater than that on surface 3 of the unimproved spool, and it is in the positive direction. Although this improvement will increase the force on surface 2, the forces in the positive direction on surface 3 and surface 4 increases more. The resultant forces on surfaces 2, 3 and 4 of the improved spool are greater than those of the unimproved spool, and the direction of the resultant forces is positive. This resultant force is opposed to the flow force and can counteract part of the flow force. So, the resultant force compensates for the flow force and is conducive to the stability of the spool. The sums of forces on surfaces 1, 2, 3 and 4 of two spools are recorded in Table 1.

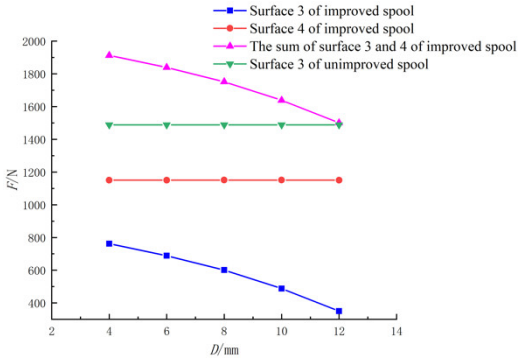

Figure 6. Forces on surfaces 3 and 4 of two spools.

Table 1. Sums of forces on all surfaces of the two spools.

D (mm)	Unimproved Spool	Improved Spool
4	−17.80	−5.78
6	−17.80	−5.36
8	−17.80	−5.25
10	−17.80	−5.44
12	−17.80	−5.45

It can be seen from Figure 7 that changing the diameter *D* has little effect on the jet angle. When *D* changes within 4–12 mm, the difference between the maximum and minimum jet angle is only 1.3°. Therefore, when changing the diameter, the flow force is mainly compensated for by the resultant forces on surfaces 2, 3 and 4. The variation of flow force with *D* is shown in Figure 8. With the decrease of diameter, the flow force first decreases and then increases. When *D* = 8 mm, the flow force is least, which is −5.25 N.

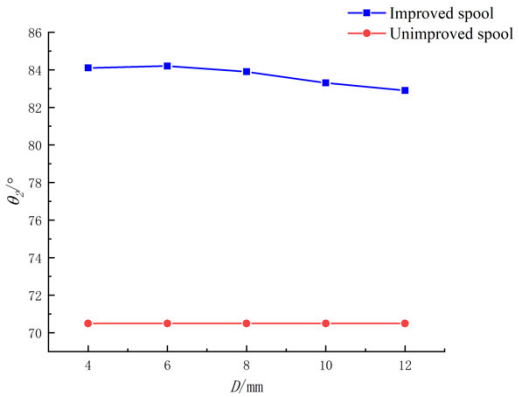

Figure 7. Jet angle of two spools.

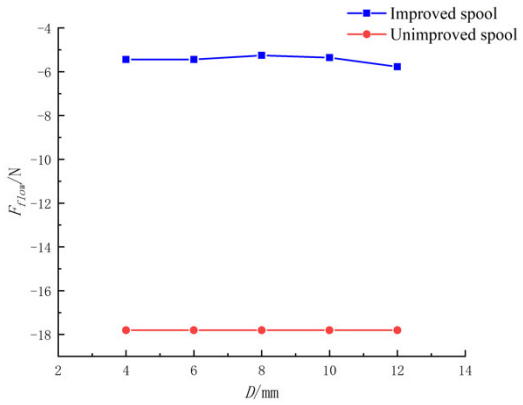

Figure 8. Flow force of two spools.

4.2. When D_1 and D Remain Unchanged, the Influence of H Change on Flow Force

When the fixed values D_1 = 16 mm, D = 8 mm, spool opening x_v = 1 mm are unchanged, H changes within a range of 2–6 mm, and every 1 mm is a measuring point. As can be seen from Figure 9, when H increases, the force on surface 1 basically remains unchanged, and the difference is only 0.59 N compared with the unimproved spool. The reason for this is the same as in the above analysis. As shown in Figure 10, since changing H does not affect the spatial distribution of surface 2, the force on surface 2 remains basically unchanged.

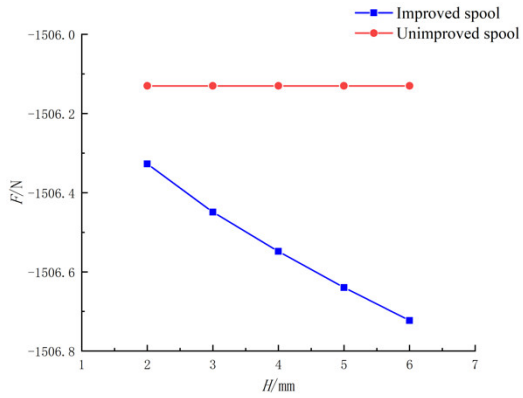

Figure 9. Force on surface 1 of two spools.

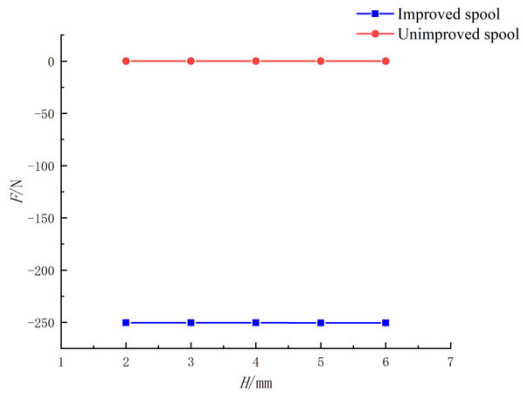

Figure 10. Force on surface 2 of two spools.

As H increases, the included angle between surface 3 and the horizontal plane decreases, and the impact of liquid flow on surface 3 decreases, resulting in a small increase in force on surface 3, as shown in Figure 11. As the included angle between surface 4 and the horizontal plane becomes smaller, the liquid flows to surface 4 after the diverting effect of

surface 3; the impact effect on surface 4 increases, as does the force on surface 4, as shown in Figure 12. As can be seen from Figure 13, as *H* increases, the reverse flow angle of the liquid flowing through surface 4 increases, and the reversed, diverting effect of surface 4 increases. The liquid flowing in the negative direction reverses the liquid flowing in the positive direction, resulting in an increased jet angle at the outlet.

As shown in Figure 14, the jet angle of the improved spool is significantly larger than that of the unimproved spool. The relationship between the jet angle and *H* is shown in Figure 15. As the jet angle increases, the flow force decreases, and the change of flow force is shown in Figure 16.

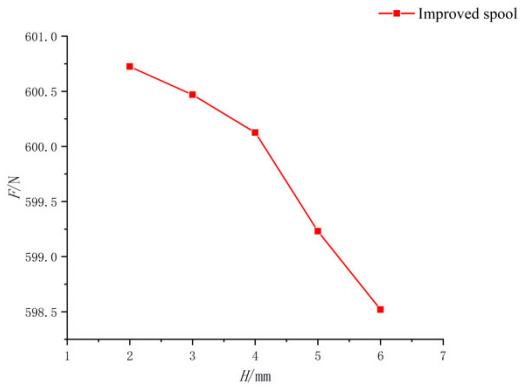

Figure 11. Force on surface 3 of the improved spool.

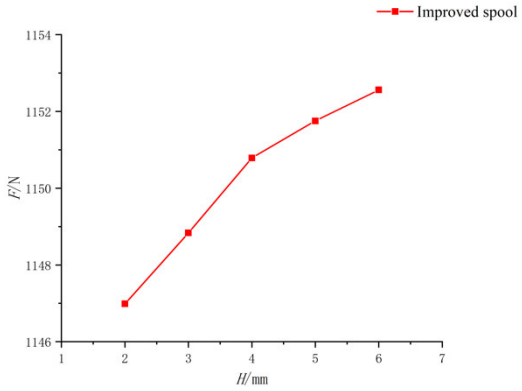

Figure 12. Force on surface 4 of the improved spool.

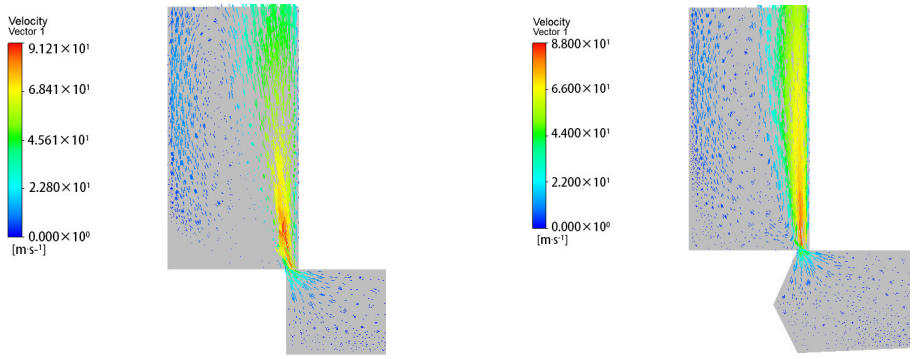

(**a**) (**b**)

Figure 13. *Cont.*

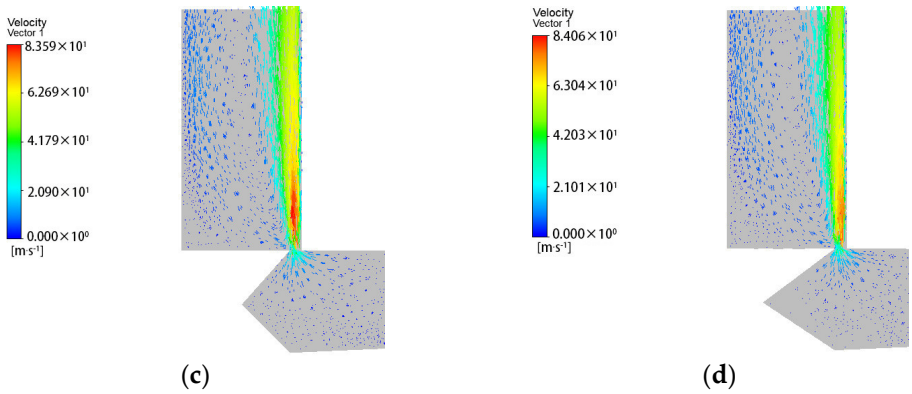

Figure 13. Velocity vector diagram. (**a**) H = 0 mm; (**b**) H = 2 mm; (**c**) H = 4 mm; (**d**) H = 6 mm.

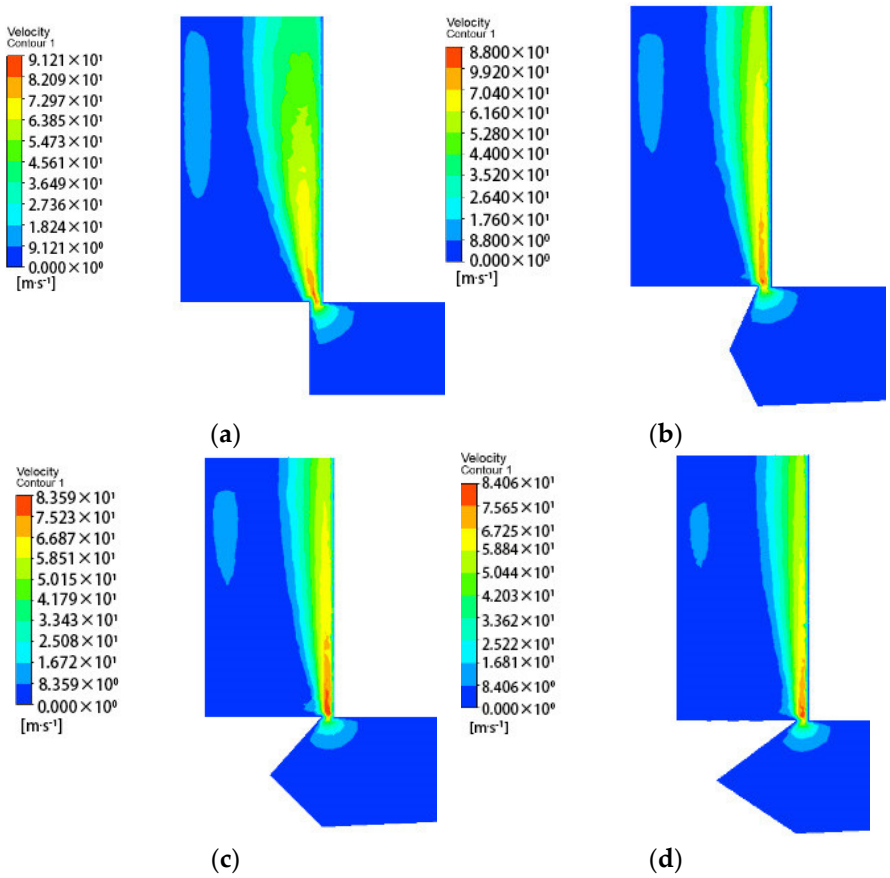

Figure 14. Velocity nephogram. (**a**) H = 0 mm; (**b**) H = 2 mm; (**c**) H = 4 mm; (**d**) H = 6 mm.

4.3. When H and D Remain Unchanged, the Influence of D_1 Changes the Flow Force

When the fixed values H = 4 mm, D = 8 mm, spool opening x_v = 1 mm are unchanged, D_1 changes within a range of 14–22 mm, and every 2 mm is a measuring point. As can be seen from Figure 17, when D_1 becomes larger, the force on surface 1 basically remains unchanged. Compared with the unimproved spool, the difference is only 0.74 N, and the reason for this is the same as in the above analyses. Since changing D_1 does not affect the spatial distribution of surface 2, it can be seen from Figure 18 that the force on surface 2 remains basically unchanged.

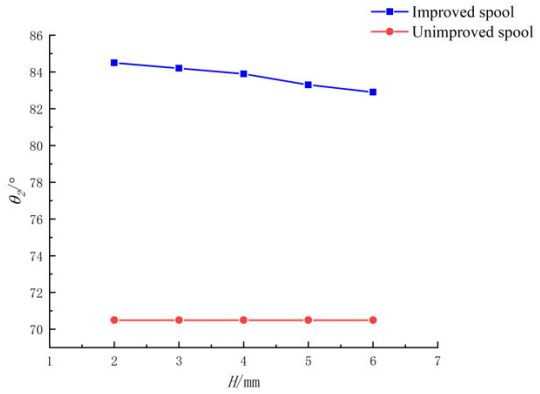

Figure 15. Jet angles of two spools.

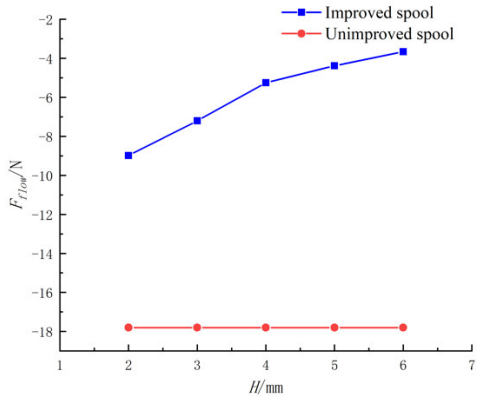

Figure 16. Flow forces of two spools.

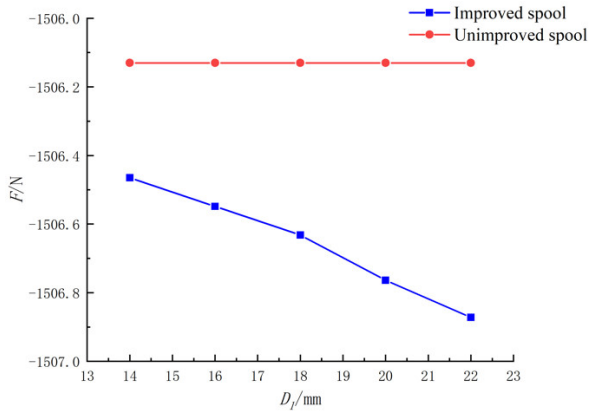

Figure 17. Force on surface 1 of the two spools.

With the increase of D_1, the included angle between surface 3 and the horizontal plane becomes larger, the impact of the liquid flow on surface 3 increases and the force on surface 3 increases, as shown in Figure 19. As can be seen in Figures 20 and 21, with the increase of D_1, the included angle between surface 4 and the horizontal plane decreases, the force along the positive direction generated by the liquid flow impacting surface 4 decreases, the reverse diversion effect of surface 4 increases within a certain range and the jet angle also increases.

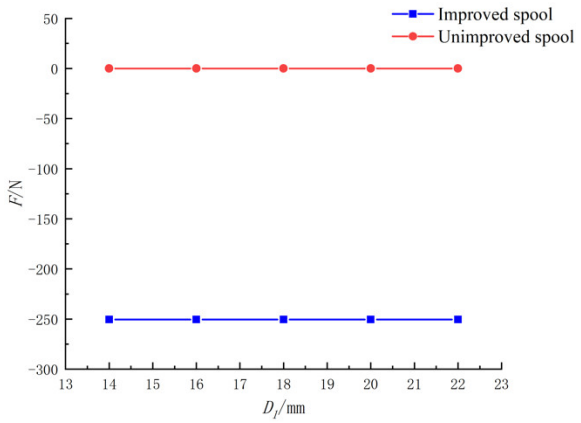

Figure 18. Force on surface 2 of the two spools.

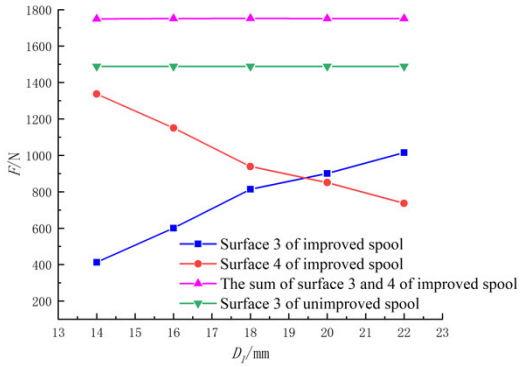

Figure 19. Force on surface 3 and 4 of the two spools.

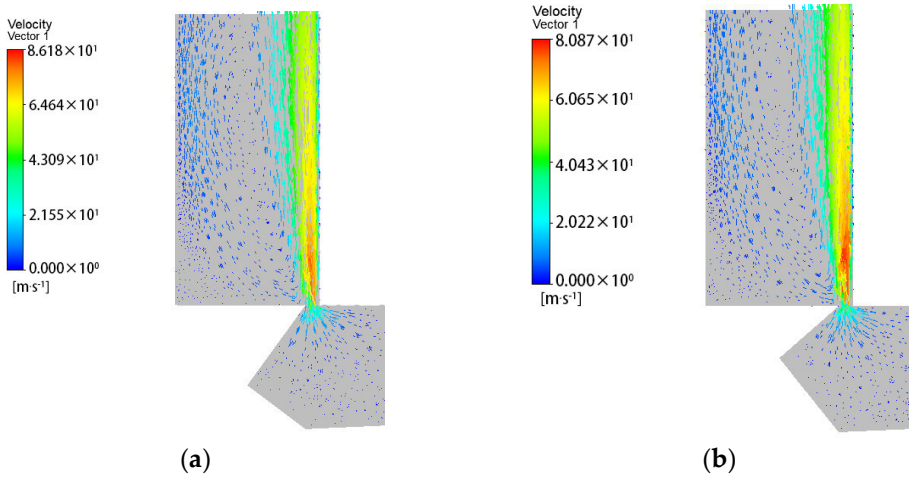

(**a**) (**b**)

Figure 20. Velocity vector diagram. (**a**) D_1 = 14 mm; (**b**) D_1 = 18 mm.

Although the force in the negative direction on surface 2 of the improved spool becomes larger, it can be seen, in Figure 19, that the sum of the forces on surface 3 and surface 4 of the improved spool is larger than that on surface 3 of the unimproved spool, both in the positive direction, and the resultant forces on surfaces 2, 3 and 4 of the improved spool are larger than those of the unimproved spool, which produces a compensatory effect. It can be seen from Figure 22 that the flow force first increases with the increase of D_1, and the minimum flow force is generated near D_1 = 18 mm, which then decreases slightly. This is because when D_1 is too large, the included angle between surface 4 and the horizontal plane is too small; the force in the positive direction generated by the liquid flow impacting

surface 4 becomes smaller, and the decrease is greater than the increase of the force on surface 3. Thus, the sum of the forces on surface 3 and surface 4 becomes smaller. When the angle between surface 4 and the horizontal plane is too small, the reversed, diverting effect of surface 4 is weakened, and the jet angle increases slowly or even decreases. The relationship between jet angle and D_1 is shown in Figure 23.

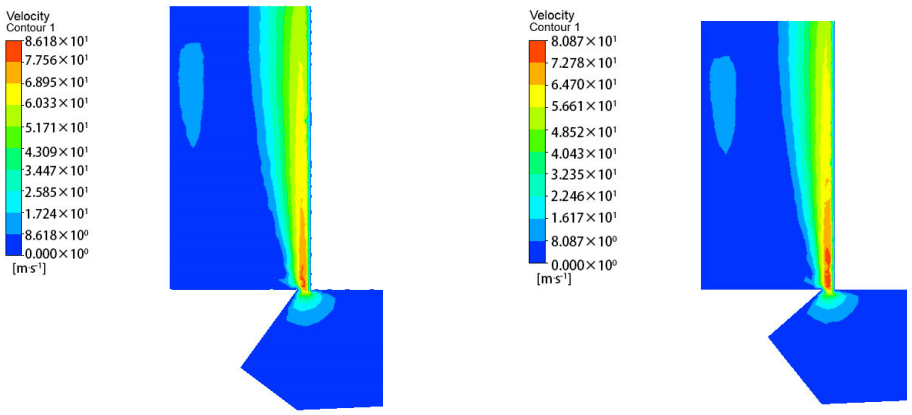

Figure 21. Velocity nephogram. (**a**) D_1 = 14 mm; (**b**) D_1 = 18 mm.

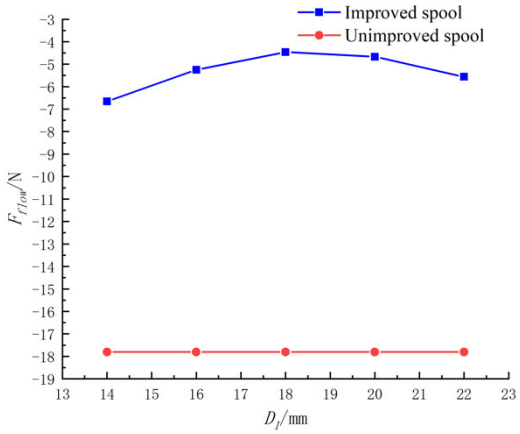

Figure 22. Flow forces of the two spools.

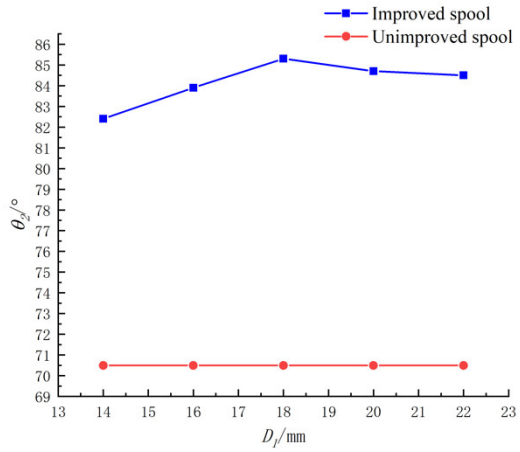

Figure 23. Jet angles of the two spools.

5. Experimental Verification

The testbed consisted of a driving device, force sensor, data acquisition card, pressure gauge, displacement sensor, solenoid valve, accumulator, relief valve, hydraulic pump and throttle valve. The hydraulic circuit is shown in Figure 24 and the testbed is shown in Figure 25. The improved spool and unimproved spool are shown in the Figure 26.

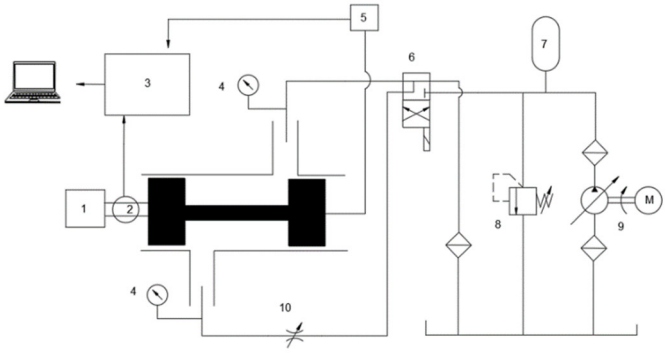

Figure 24. Hydraulic circuit. (**1**) Driving device, (**2**) force sensor, (**3**) data acquisition card, (**4**) pressure gauge, (**5**) displacement sensor, (**6**) solenoid valve, (**7**) accumulator, (**8**) relief valve, (**9**) hydraulic pump, (**10**) throttle valve.

Figure 25. Test bed.

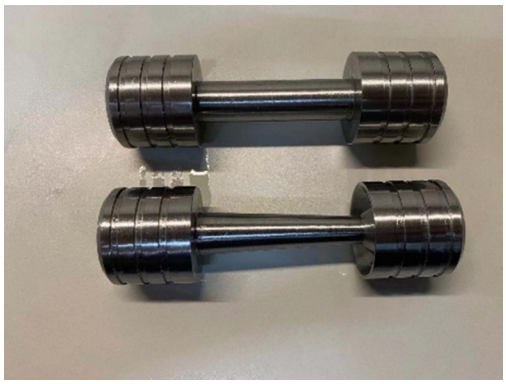

Figure 26. Improved spool and unimproved spool.

Figures 27–29 show the change of flow force with the spool opening under different inlet and outlet pressure differences. The flow force increased greatly with increasing opening. Compared with the unimproved spool, the flow force of the improved spool is significantly reduced. With the increase of the opening, the decrease in flow force of the improved spool is more obvious.

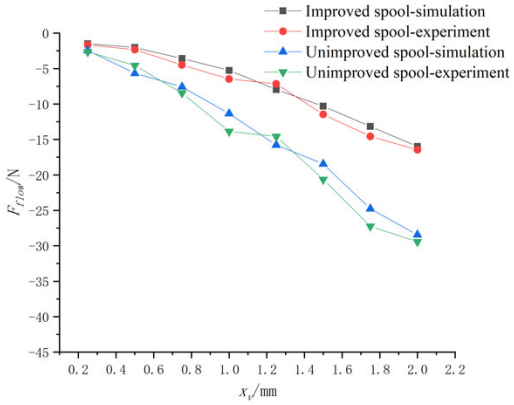

Figure 27. Flow force at 1.5 MPa.

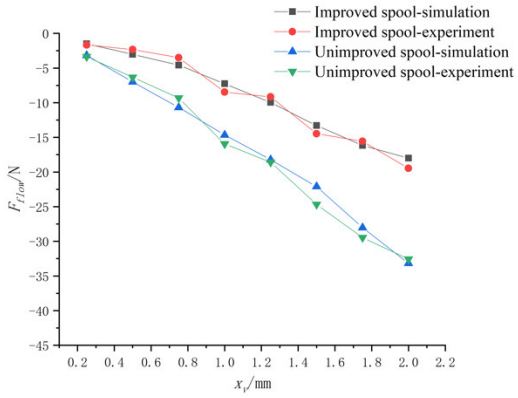

Figure 28. Flow force at 2.5 MPa.

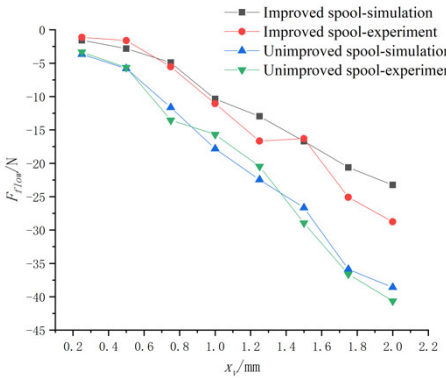

Figure 29. Flow force at 3.5 MPa.

In order to quantitatively study the flow-force compensation of the improved spool, the compensation coefficient γ is defined as the flow-force increment per spool opening, and γ can be expressed as follows:

$$\gamma = \frac{\Delta F_{flow}}{\Delta x_v} \tag{15}$$

Obviously, when $\gamma > 0$, it indicates that the flow force is completely offset and produces a flow force in the opposite direction, that is, it produces over-compensation. When $\gamma = 0$, it indicates that the flow force is completely offset. When $\gamma < 0$, it means that part of the flow force is compensated for; and, the smaller the absolute value of γ, the more the flow force is compensated for, and the more stable is the compensation characteristic.

The flow forces under different pressure difference were fitted to the spool opening to obtain various compensation coefficients, as shown in Table 2. With the increase of pressure difference, the absolute values of γ for the two spools became larger, the compensation effect decreased, and the compensation characteristic became unstable. However, at the same pressure difference, the absolute value of the compensation coefficient of the improved spool was less than that of the unimproved spool. When the pressure difference was 1.5 MPa, the absolute value of the compensation coefficient of the improved spool was 53.3% lower than that of the unimproved spool. When the pressure difference was 3.5 MPa, the absolute value of the compensation coefficient of the improved spool was 36.5% lower than that of the unimproved spool; the compensation effect is more obvious in the case of small pressure differences.

Table 2. Compensation coefficients.

Pressure Difference (MPa)	Unimproved Spool	Improved Spool
1.5	−6.3	−13.5
2.5	−8.9	−17.5
3.5	−12.2	−19.2

6. Conclusions

In this paper, an improved scheme was proposed to reduce flow force. We reduced the diameter of one side of a spool stem to make shape it into a round platform. A triangular groove was circumscribed on the step of the same side, which could control the flow direction of the fluid. This increased the jet angle at the outlet and reduced the flow force. As the diameter of one side of the spool stem was reduced, the space on this side of the spool stem was also increased, such that more liquid flow could be guided through the triangular groove, further reducing the flow force.

Further, by analyzing the structural parameters of the spool, we concluded that:

(1) When fixed, H and D_1 remained unchanged and D became smaller, the flow force first decreased and then increased. When D = 8 mm, the flow force in the negative direction was the smallest.

(2) When fixed, D and D_1 remained unchanged; with increasing H, the jet angle increased, the flow force compensation effect increased and the flow force decreased, accordingly. Increasing H had a positive effect on flow-force compensation and was conducive to the stability of the spool.

(3) When fixed, D and H remain unchanged; with increasing D_1, the jet angle increased and the flow force decreased. When D_1 was too large, the jet angle increased slowly or even decreased, and the flow force increased.

Further, the flow force of the spool under different opening diameters was analyzed experimentally. The experiment results were consistent with the simulation results, which verifies the effectiveness of the improvement. The compensation coefficient was defined and calculated. The calculation results show that the absolute value of the compensation coefficient of the improved spool was less than that of the unimproved spool. The improved spool had obvious flow-force compensation characteristics. With increasing pressure difference, the absolute value of the compensation coefficients of the two spools became larger, the compensation effect decreased, and the compensation characteristic became unstable. When the pressure difference was small, the compensation effect was more apparent.

Author Contributions: Conceptualization, R.L. and X.D.; methodology, X.D.; software, X.D. and J.L. (Jilu Liu); validation, F.C., Y.C. and Q.L.; formal analysis, R.L. and X.D.; investigation, F.C.; resources, R.L., J.L. (Jianghai Lin), J.X. and F.C.; data curation, R.L., X.D. and F.C.; writing—original draft preparation, X.D.; writing—review and editing, X.D.; visualization, J.X., Y.C., and Q.L.; supervision, F.C., Y.C. and J.L. (Jilu Liu); project administration, R.L. and J.L. (Jianghai Lin); funding acquisition, R.L, J.L. (Jianghai Lin) and J.X. All authors have read and agreed to the published version of the manuscript.

Funding: Funding was obtained from the Industrial Foundation Strengthening Project of the Ministry of Industry and Information Technology of the People's Republic of China, grant number TC180A3Y1; national key R and D projects, grant number 2016YFD0701104; major innovation projects in Shandong Province, China, grant number 2019TSLH0303; key R and D plan of Shandong Province, China, grant number 2020CXGC010806; key R and D plan of Shandong Province, China, grant number 2020CXGC011005; and innovation team project of colleges and universities of Jinan science and Technology Bureau, Shandong Province, China, grant number 2020GXRC042.

Institutional Review Board Statement: Not applicable.

Informed Consent Statement: Not applicable.

Data Availability Statement: The data presented in this study are available on request from the corresponding author.

Acknowledgments: I would like to thank my tutor, Ruichuan Li, for all his support and guidance. I would like to thank my colleagues for their care and help in my daily work.

Conflicts of Interest: The authors declare no conflict of interest.

References

1. Jiang, Y.; Xu, J.M. Simulation research on dynamic performance of cartridge two position four way directional valve. *Mach. Tool Hydraul.* **2021**, *49*, 133–135.
2. Kang, J.; Yuan, C.H.; Wang, J.T. Numerical study on hydrodynamic oscillation and forced vibration in front stage of pressure servo valve. *J. Vib. Shock* **2021**, *40*, 120–128.
3. Chen, L.J.; Peng, Z.Y.; Gao, W.; Ai, C. Position control of direct-acting high-frequency proportional valve. *Chin. Hydraul. Pneum.* **2021**, *2*, 36–41.
4. Yun, J.T.; Jiao, Z.X.; Wu, S. Design and simulation of high-flow high-speed on/off valve driven by piezoelectric. *J. Mech. Eng.* **2020**, *56*, 226–234.
5. Choi, J.; Ahn, J.H.; Kim, H.Y. Modeling the dynamic behavior of a pilot-operated solenoid valve for an ultra-high pressure vessel. *Appl. Sci.* **2021**, *11*, 2329. [CrossRef]
6. Yan, H.; Li, J.; Cai, C.; Ren, Y. Numerical investigation of erosion wear in the hydraulic amplifier of the deflector jet servo valve. *Appl. Sci.* **2020**, *10*, 1299. [CrossRef]
7. Fan, S.; Xu, R.; Ji, H.; Yang, S.; Yuan, Q. Experimental investigation on contaminated friction of hydraulic spool valve. *Appl. Sci.* **2019**, *9*, 5230. [CrossRef]
8. Lee, S.Y.; Blackburn, J.F. Contributions to hydraulic control: Steady-state axial forces on control-V alve pistons. *Trans. ASME* **1952**, *74*, 1005–1011.
9. Amirante, R.; Vescovo, R.D.; Lippolis, A. Flow forces analysis of an open center hydraulic directional control valve sliding spool. *Energy Convers. Manag.* **2006**, *47*, 114–131. [CrossRef]
10. Amirante, R.; Catalano, L.A.; Poloni, C.; Tamburrano, P. Fluid-dynamic design optimization of hydraulic proportional directional valves. *Eng. Optim.* **2014**, *46*, 1295–1314. [CrossRef]
11. Rannow, M.B.; Li, P.Y. Soft switching approach to reducing transition losses in an on/off hydraulic valve. *ASME J. Dyn. Syst. Meas. Control* **2012**, *134*, 064501. [CrossRef]
12. Ye, Y.; Yin, C.B.; Li, X.D.; Zhou, W.J.; Yuan, F.F. Effects of groove shape of notch on the flow characteristics of spool valve. *Energy Convers. Manag.* **2014**, *86*, 1091–1101. [CrossRef]
13. Lu, Q.Q.; Tiainen, J.; Kiani-Oshtorjani, M.; Wu, Y.F. Lateral force acting on the sliding spool of control valve due to radial flow force and static pressure. *IEEE Access* **2021**, *9*, 126658–126669. [CrossRef]
14. Lu, Q.Q.; Tiainen, J.; Kiani-Oshtorjani, M.; Ruan, J. Radial flow force at the annular orifice of a two-dimensional hydraulic servo valve. *IEEE Access* **2020**, *8*, 207938–207946. [CrossRef]
15. Lu, X.B.; Peng, J.H.; Li, S.J. Dynamic characteristics of the jet force on the flapper of the pilot stage in a flapper nozzle servo valve under the flow-solid interaction. *J. Beijing Inst. Technol.* **2020**, *29*, 445–455.
16. Lu, Q.Q.; Ruan, J.; Li, S. Study on steady-state flow force of pilot helical orifice of 2D servo valve. *Fluid Mach.* **2019**, *47*, 25–30.
17. Wang, H.; Jia, W.H.; Zhu, Y.R.; Sun, C.L.; Wang, C. Dynamic characteristics and stability analysis of poppet relief valve. *Mach. Tool Hydraul.* **2019**, *47*, 144–147.
18. Qu, D.H.; Zhou, Y.S.; Luo, W.; Liu, Y.F.; Fu, B. Influences of fit clearances on steady-state fluid forces of relief valves. *China Mech. Eng.* **2018**, *29*, 893–899.
19. Zhang, S.F.; Zhang, S.; Wang, Q.; He, X.H.; Xu, L. Transient properties of hydraulic operated directional valve based on fluid-structure interaction. *J. Ordnance Equip. Eng.* **2017**, *38*, 151–155.
20. Herakovic, N.; Duhovnik, J.; Simic, M. CFD simulation of flow force reduction in hydraulic valves. *Tech. Gaz.* **2015**, *22*, 453–463. [CrossRef]

21. Altare, G.; Rundo, M.; Olivetti, M. 3D dynamic simulation of a flow force compensated pressure relief valve. In Proceedings of the ASME 2016 International Mechanical Engineering Congress and Exposition, Phoenix, AR, USA, 11–17 November 2016; Volume 7, pp. 11–17.
22. Tan, L.; Xie, H.B.; Chen, H.B.; Yang, H.Y. Structure optimization of conical spool and flow force compensation in a diverged flow cartridge proportional valve. *Flow Meas. Instrum.* **2019**, *66*, 170–181. [CrossRef]
23. Roberto, F.; Massimo, R. Numerical and experimental investigation on a conical poppet relief valve with flow force compensation. *Int. J. Fluid Power* **2017**, *18*, 111–122.
24. Zhang, Y.J.; Li, W.L. Compensation of steady state flow forces in slide valves. *J. Heilongjiang Univ. Technol. (Compr. Ed.)* **2018**, *18*, 51–55.
25. Dong, Y.K.; Fu, L.D. Structural simulation analysis of spool valve with V-shaped throttle groove. *J. Wuhan Univ. Sci. Technol.* **2021**, *44*, 119–124.